

**Electron-hole liquid formation in formamidinium lead bromide perovskite  $FAPbBr_3$** Giuseppe Ammirati <sup>1,2</sup>, Daniele Catone <sup>1</sup>, Patrick O’Keeffe <sup>3</sup>, Francesco Toschi <sup>1</sup>, Stefano Turchini <sup>1</sup>,  
Fabio Matteocci <sup>2</sup>, Jessica Barichello <sup>2</sup>, Aldo Di Carlo <sup>1,2</sup> and Faustino Martelli <sup>4,\*</sup><sup>1</sup>*Istituto di Struttura della Materia—CNR (ISM-CNR), EuroFEL Support Laboratory (EFSL),**Via del Fosso del Cavaliere 100, 00133 Rome, Italy*<sup>2</sup>*CHOSE, University of Rome “Tor Vergata”, Rome 00133, Italy*<sup>3</sup>*Istituto di Struttura della Materia—CNR (ISM-CNR), EuroFEL Support Laboratory (EFSL), Monterotondo Scalo 00015, Italy*<sup>4</sup>*Istituto per la Microelettronica e i Microsistemi (IMM) CNR, Rome 00133, Italy*

(Received 19 July 2023; revised 10 October 2023; accepted 17 October 2023; published 6 November 2023)

We observe radiative recombination from an electron-hole liquid (EHL) in a thin film of  $FAPbBr_3$ , a metal halide perovskite used in transparent photovoltaics and light emitters. Photoluminescence (PL) at low excitation intensity and low temperatures only shows the free-exciton (FE) signal. As the excitation intensity increases, two additional signals in PL emerge: the electron-hole plasma (EHP) and the EHL recombination bands. For both the FE-EHP and the EHP-EHL phase transitions, a critical carrier density is established and a phase diagram is presented.

DOI: [10.1103/PhysRevB.108.195201](https://doi.org/10.1103/PhysRevB.108.195201)**I. INTRODUCTION**

In semiconductors, optical excitation at low fluences usually generates an ensemble of electron-hole pairs which form a noninteracting gas of excitons, usually called free excitons (FEs). Upon increasing the intensity of the optical excitation, because of the increasing dielectric screening of the Coulomb potential, excitons will tend not to form in favor of a gas of free electrons and holes, usually called an electron-hole plasma (EHP). This paradigm is the essence of the Mott transition [1], which predicts the existence of an insulator-metal transition at the so-called Mott density. Experimental evidence for the exciton-plasma Mott transition was given in silicon by Shah *et al.* [2]. Furthermore, the renormalization effect of the electronic eigenstate in the EHP results in the formation of an electron-hole liquid (EHL) state below some critical temperature [3,4]. In analogy to the real gas case, this physical picture predicts a phase separation between the EHL and the surrounding gas of both excitons and free carriers. In contrast to EHP, the EHL shows incompressibility, surface tension, and short-range order like a classical liquid. The EHL has been observed at high-intensity optical excitations in materials having long carrier lifetimes such as silicon [2,5,6], germanium [7,8], diamond [9–11], and GaP [12] as well as in bidimensional metal dichalcogenides [13,14]. While a cryogenic temperature is required for three-dimensional materials, the strong electron confinement existing in two-dimensional materials allows the observation of EHL even at room temperature.

The physics of EHPs and EHLs are fascinating from a fundamental point of view, but their study also helps us understand the fundamental properties of the materials in which they are observed, and they have implications for use in

applications, particularly as light emitters. In this context, metal halide perovskites (MHPs), which are extensively used in photovoltaic applications [15], in part thanks to the long lifetime of photoexcited carriers, can be a class of materials where the observation of electron-hole condensation could be expected. In this paper, we have chosen a material that finds applications in transparent photovoltaics [16,17] and light emitters [18,19], namely, formamidinium (FA) lead bromide ( $FAPbBr_3$ ), where the FA  $[CH(NH_2)_2]^+$  is the organic cation [20]. This material possesses a FE with a binding energy of  $\sim 25$  meV [21] and a carrier lifetime of tens to hundreds of nanoseconds [18,22] (see Fig. S1 in the Supplemental Material for our result [23]). In this paper, we present photoluminescence (PL) measurements on thin films of pure  $FAPbBr_3$  as a function of temperature and excitation intensity and provide evidence for the formation of an EHL up to temperatures of  $\sim 100$  K. A tentative phase diagram that includes the exciton-plasma Mott transition and the formation of EHL is also reported. We underline that EHL has been investigated in semiconductors with highly crystalline structure since defects reduce the lifetime of the carriers, thus hampering the formation of EHL. Herein, we report the formation of the EHL phase for a material where defects are not negligible. This important feature confirms the defect tolerance of MHPs [24–26]. In this paper, we provide fundamental insight into the optical properties of  $FAPbBr_3$  and contribute to the understanding of the behavior of excitons and free carriers in perovskites, a topic on which there are models that are in disagreement with the Mott transition [27] which lead to contradictory results [28].

**II. EXPERIMENTAL**

The sample has been prepared as follows: 1.3 M  $FABr$  (Dyesol) and 1.3 M  $PbBr_2$  (TCI) were weighed in a vial and

\*faustino.martelli@cnr.it

dissolved in DMSO. The  $FAPbBr_3$  solution was left to stir for 8 h. Here,  $2.5 \times 2.5$  cm shaped glasses (1 mm thick) were first washed with a soap:water solution (5:100 in vv) and then rinsed with distilled water and isopropanol through ultrasonic baths of 10 min to remove organic impurities and dust from the substrates. Cleaned substrates undergo an ultraviolet light soaking treatment for 30 min to improve wettability for reaching a uniform layer deposition.  $FAPbBr_3$  has been deposited under a  $N_2$  atmosphere. Before perovskite deposition, the substrates were heated to  $60^\circ C$ , and 80  $\mu L$  of the solution were dropped and spun at 4000 rpm on the hot sample for 20 s. Ten seconds after the beginning of the spin, 200  $\mu L$  of ethyl acetate was added to help the perovskite crystallization. The samples were then annealed at  $80^\circ C$  for 10 min.

PL has been measured using the output at 500 nm ( $\approx 2.5$  eV) of an optical parametric amplifier (OPA, Opera Solo, Coherent) with a pulse width duration of  $\sim 40$  fs. The OPA is pumped by a Ti:sapphire regenerative amplifier (Legend Elite, Coherent) operating at a repetition rate of 1 kHz, 35 fs of pulse duration, and 4 W power centered at 800 nm. The exciting beam was focused on the sample with a spot of  $\sim 100$   $\mu m$  diameter. A long-pass filter with the cutoff edge at 520 nm has been used to selectively eliminate the 500 nm light scattered by the sample. The PL signal was detected with a Peltier-cooled charge-coupled device camera after having been dispersed in a 30-cm-long monochromator with a 1200 grooves/mm grating. PL spectra were recorded at selected temperatures in the 12–100 K range by cooling the sample with a closed-loop He cryostat. The photoexcited carrier density  $n_0$  has been estimated using the following formula [29]:

$$n_0 = \frac{F}{\hbar\omega} \cdot \frac{A}{d},$$

where  $\hbar\omega$  is the laser photon energy,  $A$  is the absorptance approximated to 0.5 (see Fig. S2 in the Supplemental Material [23]), and  $d$  is the sample thickness (200 nm). The measurements were performed for different incident laser fluences ( $F$ ) ranging from 13 to 1020  $\mu J/cm^2$ , which give rise to carrier densities ranging from  $8.0 \times 10^{17}$  to  $6.4 \times 10^{19} cm^{-3}$ . The carrier density obtained in this way overestimates the true value because a homogeneous light intensity is considered over the whole sample thickness and laser spot diameter.

We have noticed the dramatic increase of defect-related luminescence after a temperature cycle. Therefore, all measurements were started at low  $T$  (12 K) after having checked the sample quality using the defect-related emission, and then the temperature was raised. The main reason we have used several samples is the thermal fragility of the samples, which should be considered when research on MHPs is carried out at low temperatures.

For these reasons, in this paper, we changed the samples after we cooled them to 12 K and heated them back to room temperature.

### III. RESULTS AND DISCUSSION

Figure 1 shows the PL spectra obtained at  $T = 20$  K [Fig. 1(a)], 40 K [Fig. 1(b)], and 100 K [Fig. 1(c)] at carrier densities of  $8.0 \times 10^{17}$ ,  $4.0 \times 10^{18}$ , and  $3.2 \times 10^{19} cm^{-3}$ . At low carrier density ( $8.0 \times 10^{17} cm^{-3}$ ) and  $T = 20$  K, we ob-

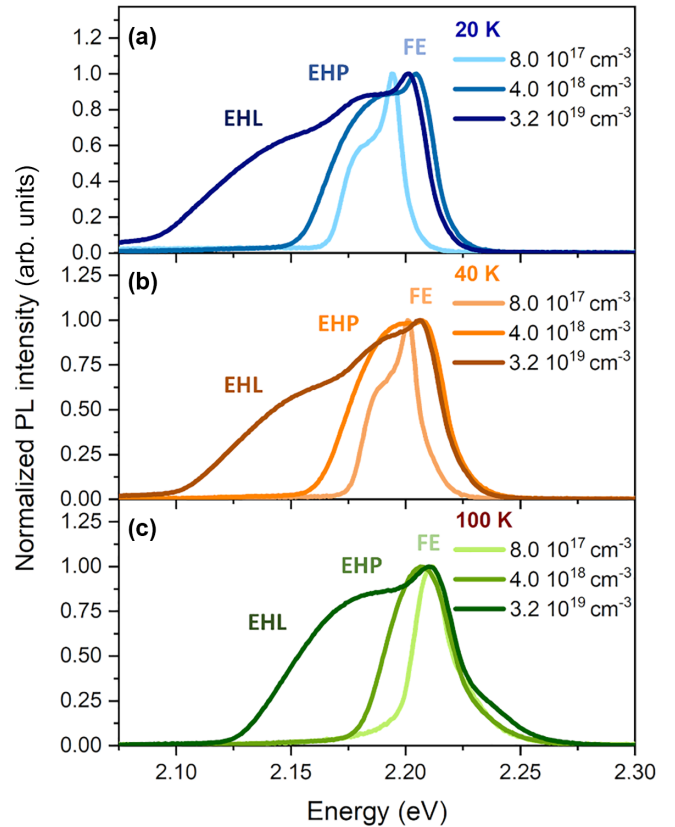


FIG. 1. Photoluminescence spectra obtained at the carrier density, respectively, of  $8.0 \times 10^{17}$ ,  $4.0 \times 10^{18}$ , and  $3.2 \times 10^{19} cm^{-3}$  and at the temperatures of (a) 20 K, (b) 40 K, and (c) 100 K.

serve the typical low-temperature PL spectrum of  $FAPbBr_3$ , with a peak centered at 2.18 eV that is attributed to the FE recombination and a shoulder (SP) at low energy that we attribute to recombination at defects [30], as this band is only visible at low temperatures and low fluences. Increasing the carrier density to intermediate values ( $4.0 \times 10^{18} cm^{-3}$ ), we see that a second broad feature appears, approximately centered at 2.20 eV, which we assign to the recombination of electron-hole pairs in an EHP. At the highest carrier density ( $3.2 \times 10^{19} cm^{-3}$ ), a third broad PL peak appears  $\sim 2.15$  eV that we assign to electron-hole recombination in an EHL. The spectral line shapes of EHP and EHL strongly depend on the temperature, with a clear broadening as the temperature decreases.

Since the line shapes of FE and EHL are independent of the carrier density, Shah *et al.* [2] suggest identifying the transition between FE and EHP (EHP and EHL) as the carrier density where the linewidth of the PL band manifests the change in its dependence on the fluence (i.e., of the carrier density) at selected temperatures. As Shah *et al.* [2] write, the choice of the half maximum as a reference point is arbitrary; a different choice of the low-energy point only shifts the numerical value of that energy. In our case, the EHP and EHL bands are difficult to distinguish in their entirety, and therefore, we have taken our reference point to be the energy difference between the FE position and that of one-fifth of the maximum PL intensity on the low-energy side of the PL spectrum band

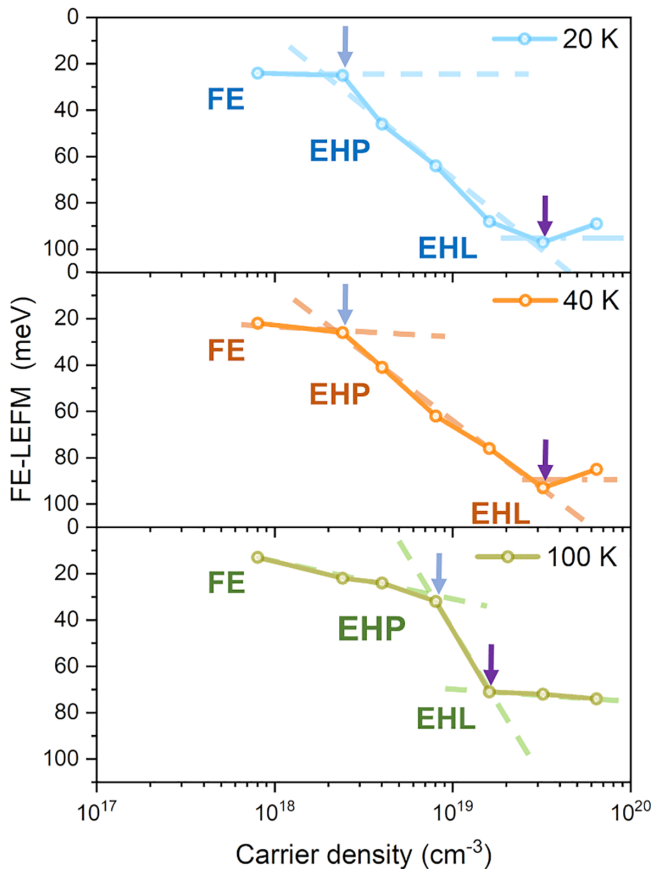


FIG. 2. Plots of the energy differences between the position of the free exciton (FE) and the low-energy full-height fifth maximum (LEFM) as a function of the photogenerated carrier density at different temperatures. The experimental points obtained at the temperatures of 20, 40, and 100 K are represented by blue, orange, and green points, respectively, while the dashed lines are a guide to the eye. Blue-gray arrows indicate the electron-hole plasma (EHP) transition, while purple arrows indicate the electron-hole liquid (EHL) transition.

(hereafter, LEFM), where at the highest excitation densities, the EHP contribution can be neglected and the signal can be safely attributed only to the EHL recombination. As can be seen in Fig. 1, the energy position of the FE is not the same in all cases. This is due to the use of several distinct samples in this paper that present some fluctuations of the FE energy due to small fluctuations of the  $FAPbBr_3$  stoichiometry, as seen in other perovskites [31] (for further details see the Experimental Section). Following the suggestion given by Shah *et al.* [2], we report on the energy difference between the FE energy and the LEFM energy of the PL band at the temperatures of 20, 40, and 100 K in Fig. 2. Following the description of Fig. 1 for increasing fluence, the FE first dissociates to form an EHP, and then at higher densities, an EHL forms. The first transition, the Mott transition, is indicated by a blue-gray arrow in Fig. 2 that represents the carrier density at which the PL spectrum starts to broaden and the FE-LEFM energy difference increases. This is due to the increase of the band-gap renormalization as the carrier density in the plasma increases [32]. Since the line shapes become constant at carrier densities higher than a

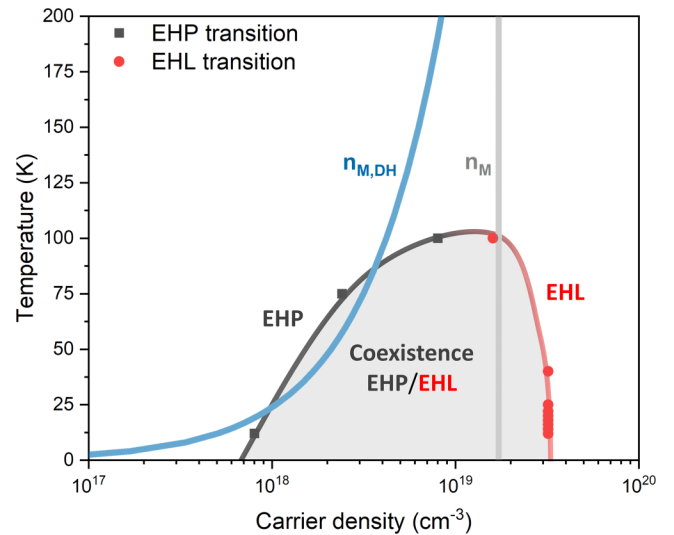


FIG. 3. Electron-hole phase diagram of  $FAPbBr_3$ , where the black squares and the red dots are our experimental data relative to the electron-hole plasma (EHP) and electron-hole liquid (EHL) formation as described in Fig. 2. The gray area indicates the coexistence area of EHP and EHL. The gray vertical line indicates the Mott density estimated with the Mott criterion, while the blue line is the theoretical curve after Eq. (2). The gray-red line is a guide to the eye for the EHP and EHL transitions.

critical value (e.g.,  $1.6 \times 10^{19} \text{ cm}^{-3}$  at 20 K), we define that carrier density as the critical density for EHL condensation (violet arrow). The critical value depends on the temperature, and this aspect will lead to a phase diagram that is reported in Fig. 3, as discussed below.

Based on our findings, we construct a phase diagram for the e-h population in  $FAPbBr_3$ . Figure 3 shows that the phase diagram reveals the stability regions of the different phases and their relative coexistence region, shedding light on the intricate carrier phase transition of the material. The plasma side of the coexistence curve (i.e., Mott transition, gray scattered points) is determined by taking the experimental carrier density at which we observe an increase of the PL linewidth characteristic for the EHP (blue arrows in Fig. 2), while the EHP-EHL transition (red scattered points) is determined to be the carrier densities at which the linewidth stops increasing (purple arrows in Fig. 2). The experimental EHP transition lies within the range of  $10^{18}$  to  $10^{19} \text{ cm}^{-3}$  in the temperature range of 20–100 K. To have a direct comparison between the experimental data and theoretical evaluations, here, we discuss two approaches to estimate the Mott density. The most common approach is based on the qualitative criterion for the existence of bound states. In the simplest approach, the Mott density occurs when the mean exciton distance is approximately equal to the exciton Bohr radius ( $a_x$ ) [33], the so-called Mott criterion, leading to

$$n_M \approx \frac{1}{a_x^3} = \left( \frac{\mu/m_e}{a_B \epsilon_{\text{eff}}} \right)^3 = 1.6 \times 10^{19} \text{ cm}^{-3}, \quad (1)$$

where  $a_x = 3.9 \times 10^{-7} \text{ cm}$ ,  $a_B$  is the Bohr radius,  $\epsilon_{\text{eff}} = 8.42$  is the effective dielectric screening, and  $\mu/m_e = 0.115$  is the excitonic reduced mass [21]. This model is very simple and

temperature independent and usually overestimates the carrier density, as can be seen in Fig. 3, where the model prediction (gray line) is compared with the experimental data; it only grasps the order of magnitude. A more complex approach that allows for a better estimation of the Mott density defines a screening length in the Debye-Hückel approximation. The energy distributions of the carriers follow a Boltzmann distribution, and we point out that it is a delicate assumption in conditions of a degenerate carrier distribution (i.e., very low-temperature regimes) [33,34].

It follows that

$$n_M^{DH} = 0.708 \frac{kT}{a_X^3 R_y^*} \approx 4.2 \times 10^{16} \frac{\text{cm}^{-3}}{\text{K}} \cdot T(K), \quad (2)$$

where  $k$  is the Boltzmann constant,  $R_y^*$  is the exciton binding energy, and  $T$  is the temperature.

The blue line in Fig. 3 shows that the theoretical result is in good agreement with the experimental data. A more sophisticated description of the Mott density could be in principle calculated *ab initio* involving the so-called random phase approximation [35]; however, this approach is beyond the scope of this paper, which is intended to provide an experimental demonstration of EHL formation in MHPs.

The large linewidth of the PL bands of MHPs makes a quantitative analysis of results that critically depend on the linewidth analysis difficult, and this is the source of the quantitative uncertainties found in our analysis. Nevertheless, the FE-EHP and EHP-EHL phase transitions have been clearly

observed in our experiments, and fair agreement with the Mott model based on the Debye-Hückel approximation has been found. It will be intriguing to study in the future other MHPs with different halide composition and dimensionality to form a large set of data that will allow a better and reliable picture of the electron-hole pair physics in this important class of materials.

#### IV. CONCLUSION

In conclusion, temperature-dependent and fluence-dependent PL measurements on FA lead bromide have shed light on the Mott transition and the formation of EHL in MHPs. Our experimental results have allowed us to sketch a phase diagram of the electron-hole pair system on perovskites, in which the critical carrier densities and temperature for the FE-EHP and EHP-EHL transitions have been determined.

In this paper, we open a field of research in MHPs that, with the investigation of different halide composition and dimensionality, will give clearer insight into the properties of photoexcited carriers in this technologically relevant class of materials.

#### ACKNOWLEDGMENT

We gratefully acknowledge financial support from the European Union's Horizon 2020 research and innovation programme under Grant Agreement No. 101007084.

- 
- [1] N. F. Mott, Metal-insulator transition, *Rev. Mod. Phys.* **40**, 677 (1968).
  - [2] J. Shah, M. Combescot, and A. H. Dayem, Investigation of exciton-plasma Mott transition in Si, *Phys. Rev. Lett.* **38**, 1497 (1977).
  - [3] M. Combescot and P. Nozieres, Condensation of excitons in germanium and silicon, *J. Phys. C: Solid State Phys.* **5**, 2369 (1972).
  - [4] W. F. Brinkman, T. M. Rice, P. W. Anderson, and S. T. Chui, Metallic state of the electron-hole liquid, particularly in germanium, *Phys. Rev. Lett.* **28**, 961 (1972).
  - [5] J. R. Haynes, Experimental observation of the excitonic molecule, *Phys. Rev. Lett.* **17**, 860 (1966).
  - [6] J. Shah and A. H. Dayem, Formation of electron-hole liquid in optically excited Si: Results of fast time-resolved spectroscopy, *Phys. Rev. Lett.* **37**, 861 (1976).
  - [7] C. B. à la Guillaume and M. Voos, Electron-hole drops in pure Ge, *Phys. Rev. B* **7**, 1723 (1973).
  - [8] G. A. Thomas, T. G. Phillips, T. M. Rice, and J. C. Hensel, Temperature-dependent luminescence from the electron-hole liquid in Ge, *Phys. Rev. Lett.* **31**, 386 (1973).
  - [9] R. Shimano, M. Nagai, K. Horiuchi, and M. Kuwata-Gonokami, Formation of a high  $T_c$  electron-hole liquid in diamond, *Phys. Rev. Lett.* **88**, 057404 (2002).
  - [10] N. Teofilov, R. Schliesing, K. Thonke, H. Zacharias, R. Sauer, and H. Kanda, Optical high excitation of diamond: Phase diagram of excitons, electron-hole liquid and electron-hole plasma, *Diam. Relat. Mater.* **12**, 636 (2003).
  - [11] M. Kozák, F. Trojánek, T. Popelář, and P. Malý, Dynamics of electron-hole liquid condensation in CVD diamond studied by femtosecond pump and probe spectroscopy, *Diam. Relat. Mater.* **34**, 13 (2013).
  - [12] J. Shah, R. F. Leheny, W. R. Harding, and D. R. Wight, Observation of electron-hole liquid in GaP, *Phys. Rev. Lett.* **38**, 1164 (1977).
  - [13] Y. Yu, A. W. Bataller, R. Younts, Y. Yu, G. Li, A. A. Puzosky, D. B. Geohegan, K. Gundogdu, and L. Cao, Room-temperature electron-hole liquid in monolayer MoS<sub>2</sub>, *ACS Nano* **13**, 10351 (2019).
  - [14] T. B. Arp, D. Pleskot, V. Aji, and N. M. Gabor, Electron-hole liquid in a van der Waals heterostructure photocell at room temperature, *Nat. Photon.* **13**, 245 (2019).
  - [15] A. Di Carlo, F. Bonaccorso, E. Kymakis, and T. Watson, Outdoor performance evaluation of a 2D materials-based perovskite solar farm, *Nat. Energy* **7**, 580 (2022).
  - [16] F. Matteocci, D. Rossi, L. A. Castriotta, D. Ory, S. Mejaouri, M. A. der Maur, F. Sauvage, S. Cacovich, and A. Di Carlo, Wide bandgap halide perovskite absorbers for semi-transparent photovoltaics: From theoretical design to modules, *Nano Energy* **101**, 107560 (2022).
  - [17] J. Barichello, D. Di Girolamo, E. Nonni, B. Paci, A. Generosi, M. Kim, A. Levchenko, S. Cacovich, A. Di Carlo, and F. Matteocci, Semi-transparent blade-coated FAPbBr<sub>3</sub> perovskite solar cells: A scalable low-temperature manufacturing process under ambient condition, *Sol. RRL* **7**, 2200739 (2023).

- [18] C. Hu, S. B. Shivarudraiah, H. H. Y. Sung, I. D. Williams, J. E. Halpert, and S. Yang, Discovery of a new intermediate enables one-step deposition of high-quality perovskite films via solvent engineering, *Sol. RRL* **5**, 2000712 (2021).
- [19] G. Xing, N. Mathews, S. S. Lim, N. Yantara, X. Liu, D. Sabba, M. Grätzel, S. Mhaisalkar, and T. C. Sum, Low-temperature solution-processed wavelength-tunable perovskites for lasing, *Nat. Mater.* **13**, 476 (2014).
- [20] A. Amat, E. Mosconi, E. Ronca, C. Quarti, P. Umari, Md. K. Nazeeruddin, M. Grätzel, and F. De Angelis, Cation-induced band-gap tuning in organohalide perovskites: Interplay of spin-orbit coupling and octahedra tilting, *Nano Lett.* **14**, 3608 (2014).
- [21] K. Galkowski, A. Mitioglu, A. Miyata, P. Plochocka, O. Portugall, G. E. Eperon, J. Tse-Wei Wang, T. Stergiopoulos, S. D. Stranks, H. J. Snaith *et al.*, Determination of the exciton binding energy and effective masses for methylammonium and formamidinium lead tri-halide perovskite semiconductors, *Energy Environ. Sci.* **9**, 962 (2016).
- [22] F. Zhang, B. Yang, K. Zheng, S. Yang, Y. Li, W. Deng, and R. He, Formamidinium lead bromide (FAPbBr<sub>3</sub>) perovskite microcrystals for sensitive and fast photodetectors, *Nano-Micro Lett.* **10**, 43 (2018).
- [23] See Supplemental Material at <http://link.aps.org/supplemental/10.1103/PhysRevB.108.195201> for Fig. S1, which shows the temporal decay of PL intensity at room temperature and indicates a carrier lifetime of 23 ns. Figure S2 shows transmittivity, reflectivity, and absorptance of the sample used.
- [24] K. X. Steirer, P. Schulz, G. Teeter, V. Stevanovic, M. Yang, K. Zhu, and J. J. Berry, Defect tolerance in methylammonium lead triiodide perovskite, *ACS Energy Lett.* **1**, 360 (2016).
- [25] L. Schmidt-Mende, V. Dyakonov, S. Olthof, F. Ünlü, K. M. T. Lê, S. Mathur, A. D. Karabanov, D. C. Lupascu, L. M. Herz, A. Hinderhofer *et al.*, Roadmap on organic-inorganic hybrid perovskite semiconductors and devices, *APL Mater.* **9**, 109202 (2021).
- [26] A. K. Jena, A. Kulkarni, and T. Miyasaka, Halide perovskite photovoltaics: Background, status, and future prospects, *Chem. Rev.* **119**, 3036 (2019).
- [27] V. D’Innocenzo, G. Grancini, M. J. P. Alcocer, A. R. S. Kandada, S. D. Stranks, M. M. Lee, G. Lanzani, H. J. Snaith, and A. Petrozza, Excitons versus free charges in organo-lead tri-halide perovskites, *Nat. Commun.* **5**, 3586 (2014).
- [28] S. G. Motti, M. Kober-Czerny, M. Righetto, P. Holzhey, J. Smith, H. Kraus, H. J. Snaith, M. B. Johnston, and L. M. Herz, Exciton formation dynamics and band-like free charge-carrier transport in 2D metal halide perovskite semiconductors, *Adv. Funct. Mater.* **33**, 2300363 (2023).
- [29] J. M. Richter, F. Branchi, F. Valduga de Almeida Camargo, B. Zhao, R. H. Friend, G. Cerullo, and F. Deschler, Ultrafast carrier thermalization in lead iodide perovskite probed with two-dimensional electronic spectroscopy, *Nat. Commun.* **8**, 376 (2017).
- [30] V. Campanari, A. Agresti, S. Pescetelli, A. K. Sivan, D. Catone, P. O’Keeffe, S. Turchini, A. Di Carlo, and F. Martelli, Systematic approach to the study of the photoluminescence of MAPbI<sub>3</sub>, *Phys. Rev. Mater.* **5**, 035409 (2021).
- [31] L. M. Falk, K. P. Goetz, V. Lami, Q. An, P. Fassl, J. Herkel, F. Thome, A. D. Taylor, F. Paulus, and Y. Vaynzof, Effect of precursor stoichiometry on the performance and stability of MAPbBr<sub>3</sub> photovoltaic devices, *Energy Technol. Weinh. Ger.* **8**, 1900737 (2020).
- [32] R. Zimmermann, Nonlinear optics and the Mott transition in semiconductors, *Phys. Status Solidi B* **146**, 371 (1988).
- [33] C. F. Klingshirn, *Semiconductor Optics* (Springer, Berlin, 2012).
- [34] M. A. M. Versteegh, T. Kuis, H. T. C. Stoof, and J. I. Dijkhuis, Ultrafast screening and carrier dynamics in ZnO: Theory and experiment, *Phys. Rev. B* **84**, 035207 (2011).
- [35] P. Vashishta, P. Bhattacharyya, and K. S. Singwi, Electron-hole liquid in many-band systems. I. Ge and Si under large uniaxial strain, *Phys. Rev. B* **10**, 5108 (1974).